

Artificial neural network model as a potential alternative for barometric correction of extensometric data

Gyula Mentés

Geodetic and Geophysical Institute, Research Centre for Astronomy and Earth Sciences,
Hungarian Academy of Sciences, Csatkai Endre u. 6-8, H-9400 Sopron, Hungary.
Email: mentes@ggki.hu

Abstract

The solid Earth crust is deformed by atmospheric pressure variations due to periodic and aperiodic loading. When barometric admittance is determined the local, regional or global loading effect can be calculated depending on the available pressure data. The effect of horizontally moving weather systems across the extensometric station can be taken into account with a good approximation when locally measured air pressure data before and after each individual strain data are involved into the correction. For this purpose neural networks with delayed input lines seem to be suitable. Three different neural networks were developed. All of them have delayed inputs taking six or twelve air pressure data before and after each momentary extensometric data into account to correct for remote atmospheric pressure variations on the basis of local pressure measurements. The effectiveness of the barometric pressure correction carried out by the three neural networks were investigated by tidal, Fast Fourier and coherence analyses and the results were compared with each other and with the results of simple regression methods. Tests of the neural network models show that they can be useful tools to correct extensometric data for barometric pressure and in contrast with the simple linear regression models the regional and global atmospheric effects can also be taken into account. Correction by neural networks yielded an improvement in the tidal factors relative to the correction by simple regression methods 2–5% and 30–40% in the semidiurnal and diurnal bands, respectively.

Keywords: Atmospheric pressure; Extensometer; Barometric correction; Neural network; Tidal factors

1. Introduction

Atmospheric pressure variations associated with atmospheric tides and weather changes deform the Earth in a wide frequency range (Farrell, 1972). Although the magnitude of atmospheric tides is smaller than that of ocean tide loading, the incoherent atmospheric pressure variations are the major cause of random fluctuations in local gravity and Earth deformations (Warburton and Goodkind, 1977; Spratt, 1982; Merriam, 1992; van Dam, et al., 1994, 1997, 2010; Wunsch and Stammer, 1997; Boy et al., 2006, 2009). A lot of publications deal with the correction of gravity measurements for atmospheric pressure (e.g. Niebauer 1988; Crossley et al., 1995, 2002; Neumeyer et al., 2004; Klügel and Wziontek, 2009) and with the deformation of the Earth's surface due to atmospheric variations (e.g. Rabbel and Zschau, 1985; van Dam and Wahr, 1987; van Dam et al., 1997, 2010; Latynina et al., 2003; Steffen et al., 2006; Gebauer et al., 2009, 2010). Kroner and Jentzsch (1999) summarized and compared the methods which are widely used for pressure correction. At present four methods and sometimes their combinations are used for the pressure reduction: local regression coefficient (effective admittance) applied also in the ETERNA 3.40 Earth tide data processing

program package (Wenczel, 1996); frequency-dependent admittance function (e.g. Crossley et al., 2002; Neumeyer et al., 2004); atmospheric Green's function based on local air pressure data (e.g. Niebauer, 1988); atmospheric Green's function calculated from local and regional pressure data (e.g. Spratt, 1982; van Dam and Wahr, 1987).

Correction of gravity measurement for atmospheric pressure using global (<1000 km) and regional (<50 km) pressure data yields improvement in the synoptic (days to seasonal) band, while using local pressure data improves the correction in the intertidal frequency bands down to periods of some hours, because the atmospheric pressure variations in the regional and global zones will be averaged out to some degree (Merriam, 1992; Boy et al., 1998). Front passages above the station have effects on gravity data in the semidiurnal and diurnal tidal bands (Müller and Zürn, 1983). Rabbel and Zschau (1985) showed that the shape of the horizontal strain curve is similar to the corresponding continuous pressure distribution curve, however it has opposite sign. The effect of the slowly changing global and regional pressure distributions is approximately $(-1.5)-(-2.0)\cdot 10^{-10}$ strain per hPa below the centre of the pressure anomaly while it can be disregarded in the diurnal and semidiurnal tidal bands. A discontinuous (stepwise) pressure distribution causes a nearly constant horizontal strain change with an extent of about ± 50 km from the centre of the abrupt pressure change. This is the case when the front is moving above the station. The strain leads and lags relative to pressure variation during the passage of the front. This relationship can be applied for the improvement of the correction of extensometric data for atmospheric pressure loading by local pressure data.

Gebauer et al. (2010) modelled the behaviour of the Sopronbánfalva Geodynamic Observatory (SGO) during passage of high pressure front and they found that the observatory is very sensitive to pressure fronts due its topography, namely that the steep western rock face of the observatory is perpendicular to the extensometer and the prevailing wind direction (WE) and consequently the rock deformation caused by the absorbed wind energy is parallel with the instrument. The strain shows significant changes even when the pressure front is far away from the observatory.

Tidal analysis of uncorrected strain data measured at the SGO show that the tidal amplitude factors are 10% and 40% lower than one in the diurnal and semidiurnal band, respectively. The tidal factors of strain data corrected by ETERNA are in the semidiurnal band 2–3% and in the diurnal band 10% bigger than in the uncorrected ones (Mentes, 2010; Eper-Pápai et al., 2014). These results and the investigations of Gebauer et al. (2010) suggested that better tidal factors could be obtained when regional and global air pressure data were applied for correction. To avoid the time-consuming and tiring correction by regional and global air pressure data, neural networks with delayed inputs are suggested to correct strain data by locally measured pressure data. This kind of neural networks, in contrast with the correction by a simple linear regression method, can take more air pressure data before and after the momentary strain data into account to correct strain data. The applicability of neural networks to correct strain data on the basis of local pressure measurements is investigated in this paper.

2. Neural network

The Artificial Neural Network (ANN) is a computing tool consisting of many simple elements called neurons (Fig. 1), each having the capability of recognizing underlying relationship between input and output signals. Neurons have one or more scalar inputs (x_1, x_2, \dots, x_n) which are multiplied by a scalar (w_1, w_2, \dots, w_n) and transferred to a summer to add up the weighted inputs ($x_1 \cdot w_1 + x_2 \cdot w_2, \dots, x_n \cdot w_n$). This sum is the argument of the transfer function which

produces the output ($F(x)$). Usually, ANN consists of more neurons arranged in layers. The efficiency of an ANN depends on the number of layers and neurons.

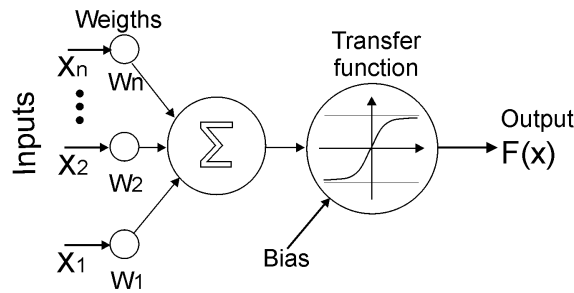


Fig. 1. A typical artificial neuron

Three different feed-forward neural networks with different complexity were developed for air pressure correction of extensometric data using the Neural Network Toolbox of Matlab (Demuth and Beale, 2001). Fig. 2 shows the simplest neural network NNW1. It consists of three layers ($l=3$, two input and an output layer) each containing four neurons ($n=4$) with seven inputs ($i=7$). In Layer#1 six inputs are for the delayed pressure data ($d=6$) and one input for the extensometric data and in Layer#2 six inputs are for the delayed extensometric data ($d=6$) and one input for the pressure data. In Layer#1 six hourly delayed pressure data are combined with each momentary extensometric data while in Layer#2 it is inverse: six hourly delayed extensometric data are combined with each pressure data. It means that twelve locally measured pressure data can be taken into account for the pressure correction of each extensometric data. The transfer functions of the neurons in the input layers of the NNW1 are “tansig” and the transfer function in the output layer is “purelin” (see the transfer functions in Fig. 2). Each neuron in the network has a bias input (b) to add a constant to the weighted inputs in order to shift the transfer function to the left by an amount of b .

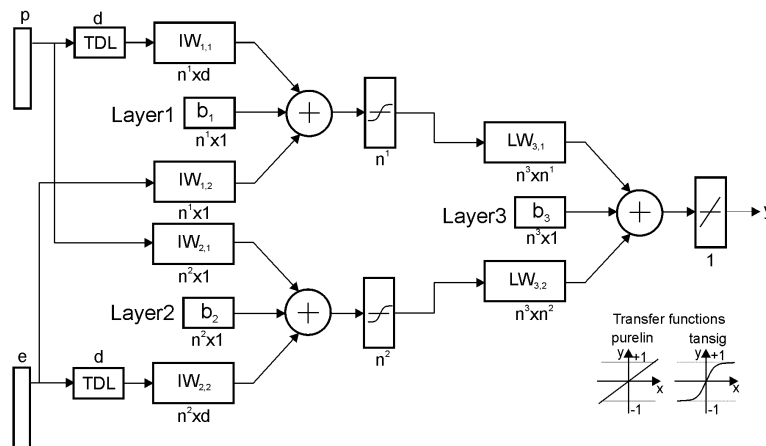


Fig. 2. Block diagram of the neural network NNW1 designed for air pressure correction of extensometric data. e and p denote extensometric and air pressure data series, respectively; d is the number of delays (hours); l is the number of layers; n^l is the number of neurons in layer l ; $IW_{l,i}$ is the weight from input i to layer l ; $LW_{l,k}$ is the weight from layer k to layer l , ($k \leq l$); y is the output.

The other two neural networks (NNW2 and NNW3) are similar to NNW1. They contain a hidden layer between the output and the input layers ($l=4$) with 13 neurons ($n=13$) in the input

and hidden layers. In Layer#1 one input is for the extensometric and twelve inputs are for the delayed ($d=12$) pressure data and in Layer#2 one input is for the pressure data and twelve inputs for the delayed extensometric data. In this case the number of the delayed inputs is twelve thus twenty four locally measured pressure data can be taken into account for the pressure correction of each extensometric data. The output layer has one neuron with 13 inputs. In NNW2 all transfer functions are “purelin”, while in NNW3 the transfer functions are “tansig” in the first three layers and “purelin” in the output layer. The output layer of each NNW has a target input (not denoted in Fig. 2). The y output signal of the NNW is compared to the target signal to get the best approach of the target during learning process of the neural network.

The neural networks were initialized by the Nguyen-Widrow layer initialization function (initnw). Widrow-Hoff weights/bias learning rule (learnwh) was used for updating the biases and weights during learning. The Levenberg-Marquardt backpropagation function (trainlm) served for training the networks, while the theoretical tide, calculated by the ETERNA for the actual year, was applied as a target function and the measured extensometric and pressure data were the input functions. During training the weights and biases of the network are iteratively adjusted to minimize the network performance function, which is the averaged squared error (mse) between the network output and the target. Error level of 10^{-3} was given as performance goal. After training the network the air pressure correction was carried out by the “sim” function, which takes the network inputs (extensometric (e) and pressure (p) data), the network parameters (weights and biases obtained during training) and returns the y output (Fig. 2).

3. Methods

Eleven years (2000–2010) extensometric data were yearly corrected for air pressure by different methods and analysed by the ETERNA 3.40 Earth tide data processing program (Wenzel, 1996) using the Wahr–Dehant Earth model (Dehant, 1987), the HW95 tidal potential catalogue (Hartmann and Wenzel, 1995) and the built-in high-pass filter with a cut-off frequency of 0.8 cpd. To compare the effectiveness of the air pressure correction by neural networks with other methods the following extensometric raw data were subjected to tidal analysis: uncorrected, corrected by linear regression model (local admittance), corrected by the ETERNA during the analysis, and data corrected by neural networks (NNW1, NNW2, NNW3). The efficiency of the air pressure correction by neural networks compared to other methods was investigated through tidal parameters from ETERNA and Fast Fourier Transformation, regression and coherence analyses of the tidal adjustment residuals.

4. Results and discussion

4.1. Results of the corrections

The training of the networks continued till the average mean square error reached a minimum value. The results can be seen in Table 1. In every case, the errors are about one order of magnitude higher than the given performance goal (10^{-3}). The training process of NNW3 produces the smallest errors and the simplest neural network NNW1 has slightly higher errors than NNW3. The smaller errors of NNW3 compared to NNW2 can probably be attributed to the non-linear transfer functions in the first three layers of NNW3 (see Demuth and Beale, 2001).

Table 1. Average mean square errors of the training

Year	NNW1	NNW2	NNW3
2000	0.047	0.057	0.016
2001	0.041	0.066	0.026
2002	0.032	0.058	0.020
2003	0.024	0.043	0.016
2004	0.018	0.031	0.012
2005	0.029	0.022	0.010
2006	0.038	0.023	0.010
2007	0.027	0.048	0.021
2008	0.061	0.031	0.013
2009	0.048	0.102	0.039
2010	0.042	0.075	0.023

Fig. 3 shows the results of tidal analysis of extensometric data corrected for air pressure by different methods, as an example, for the year 2005. Analysis results for other years are similar. All the three neural networks provide better amplitude factors (with the exception of the OO1 and M3M6 wave groups) than those calculated from the extensometric data corrected by simple regression methods. The small difference between the amplitude factors means that a good correction can be achieved. In Fig. 4 the amplitude factors of the main lunar diurnal O1 and main semidiurnal M2 tidal constituents are shown for the whole investigated period (2000–2010). The amplitude factors of O1 from the NNW3 model are nearer to the value of one than those from other methods. Correction by NNW1 produces also similar good amplitude factors as NNW3. The amplitude factors obtained by the correction with NNW3 are in every year about 0.9, while in the case of NNW1 there are nearer to one but the dispersion of the factors is high. While the amplitude factors of M2 from analysis of the corrected data by neural networks are slightly smaller than one those from the correction with simple regression methods are generally much higher than one. The situation is similar in the whole diurnal and semi diurnal band (see also Fig. 3). On the basis of tidal analysis it can be inferred that the NNW3 is more suitable for air pressure correction of extensometric data than the other two neural networks.

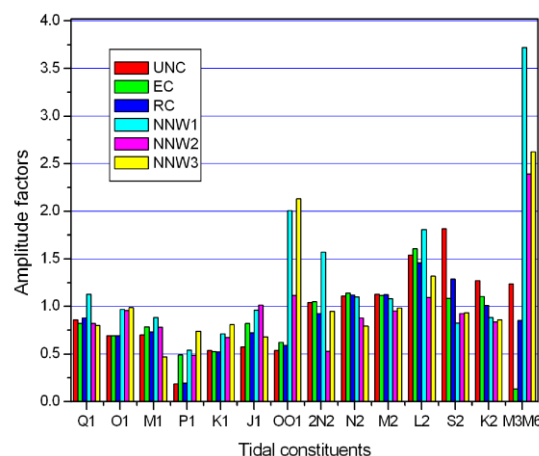


Fig. 3. Amplitude factors obtained for year 2005 from tidal analysis of extensometric data corrected by different methods. UNC is uncorrected data; EC is data corrected by ETERNA; RC is data corrected by linear regression method; NNW1, NNW2, NNW3 are data corrected by neural networks.

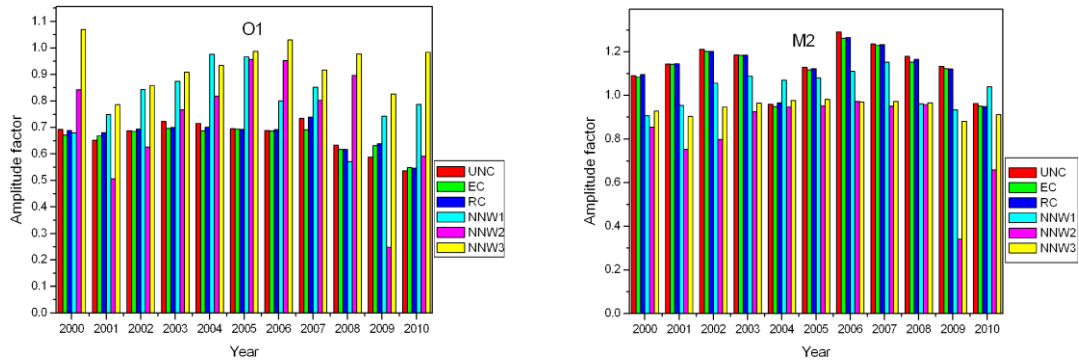


Fig. 4. Amplitude factors of the O1 and M2 tidal constituents obtained for years 2000–2010 from tidal analysis of extensometric data corrected by different methods. UNC is uncorrected data; EC is data corrected by ETERNA; RC is data corrected by linear regression method; NNW1, NNW2, NNW3 are data corrected by neural networks.

4.2. Investigation of the effectiveness of the correction

Looking at the tidal results the question arises: are the good amplitude factors due to the air pressure correction or the neural network adjusts its output data to the theoretical tide? To answer this question the residual curves from tidal analysis (the adjusted tidal components are subtracted from the measured data) were investigated.

The residual data and the local air pressure were subjected to linear regression analysis to investigate the remaining pressure data in the residuals. Since the NNW3 yielded the best amplitude factors, the regression coefficients between air pressure and the residuals from analysis of uncorrected data, corrected by ETERNA and by NNW3 were calculated. The results are summarized in Table 2.

Table 2. Regression coefficients between tidal residuals and air pressure in the case of different correction of extensometric data for air pressure

Year	Uncorrected [nstr/hPa]	Corrected by ETERNA [nstr/hPa]	Corrected by NNW3 [nstr/hPa]
2000	1.9689	0.009	0.229
2001	1.935	0.112	0.153
2002	-3.881	0.046	-0.053
2003	-3.280	0.027	0.112
2004	-4.114	0.053	0.026
2005	-3.546	0.078	0.037
2006	-3.838	-0.001	0.203
2007	-4.269	0.001	0.187
2008	-3.823	0.184	0.199
2009	-3.202	0.165	0.182
2010	-3.380	-0.014	0.049

Regression coefficients are slightly larger in the case of NNW3 than in the case of the ETERNA correction. This may be explained by the fact that the neural network takes twelve

air pressure data before and after the actual extensometric data while the ETERNA takes only each individual extensometric and pressure data into account during the correction and similarly the related pressure and residual data are used for calculation of the regression coefficients. To investigate this assumption the amplitude spectrum of the residuals and the air pressure were calculated (Fig. 5). It can be seen that the spectral amplitudes from the NNW3 correction in the diurnal and semidiurnal frequency ranges are about the half of the amplitudes obtained by the tidal analysis of uncorrected extensometric data (UNC) and data corrected by ETERNA (EC).

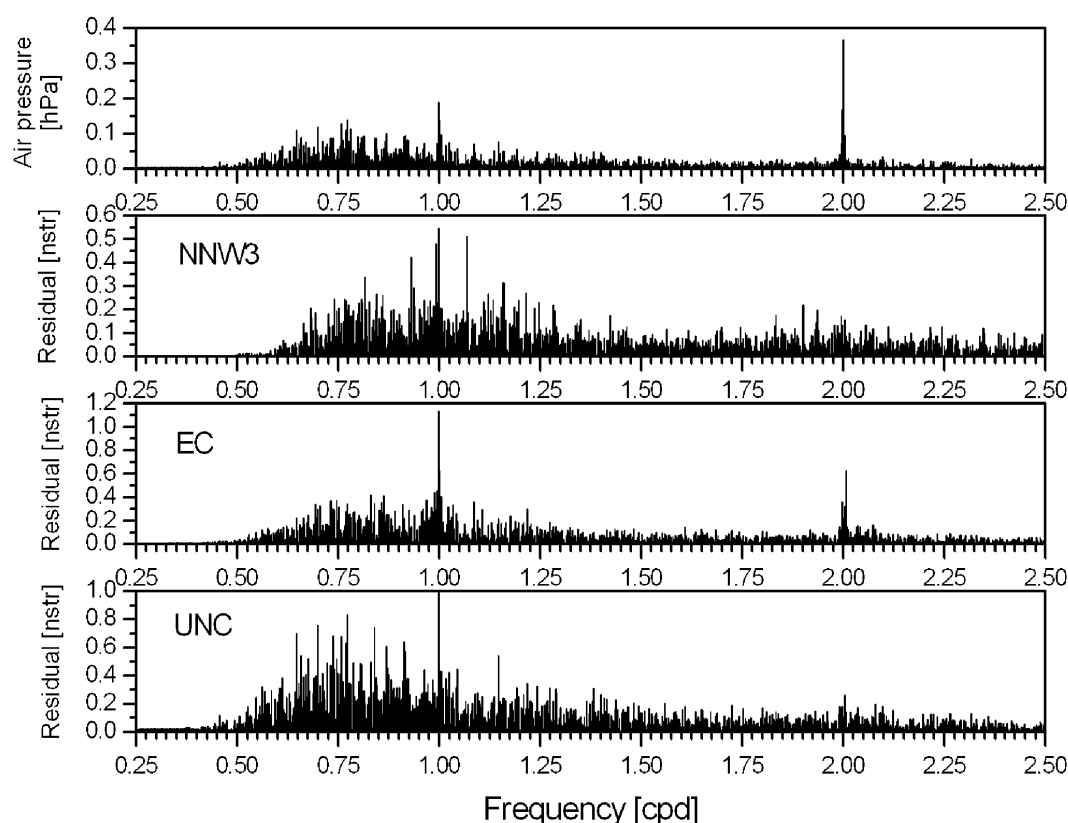


Fig. 5. Amplitude spectrum of the air pressure data, the residuals of tidal analysis of the uncorrected extensometric data (UNC), data corrected by ETERNA (EC), and data corrected by neural network (NNW3).

The coherence analysis between pressure and residual data (Fig. 6) also shows that the neural network eliminates the air pressure effect in the whole frequency range while the correction by the ETERNA decreases it only in the diurnal and semidiurnal frequency domains. Fig. 7 shows the coherence between the theoretical tide and the uncorrected extensometric data as well as extensometric data corrected by different methods (EC, NNW2 and NNW3). While correction by ETERNA improves the coherence, the neural networks decrease it. It is somewhat inconsistent with the former findings. The coherence between two signals is low when the signals are nonlinear, either there is a phase shift between the signals or the signals have high noise (Formenti, 1999). The transfer functions of NNW2 are linear (“purelin”). The coherence functions of NNW2 and NNW3 are similar which means that the non-linear transfer functions in the first three layers of NNW3 do not cause signal non-linearity during the correction. The noises are in the same order in the case of all corrections, so we can assume that the noise cannot cause the coherence results of Fig. 7. The phase shifts

of the O1 and M2 tidal waves from the uncorrected data are -5 and -13 degrees, respectively. Both neural networks change these phases into -70 degrees. Phases of other waves are practically unchanged. It can be inferred that this phase shift causes the lower coherence in the diurnal and semi diurnal band in the case of the neural networks. In contrast with this, the correction by ETERNA changes the phases of P1 and K2 significantly (by about 130 degree) and leaves the phases of O1 and M2 unchanged compared to the uncorrected data. The coherence here is better than the coherence between the theoretical tide and uncorrected extensometric data (Fig. 7). This result queries the assumption that the phase shifts decrease the coherence but this question needs further investigations. The lower coherence in the case of the extensometric data corrected by neural networks hints to the characteristic of the neural network that it does not tend to fit the measured data to the target function (theoretical tide) during the correction procedure.

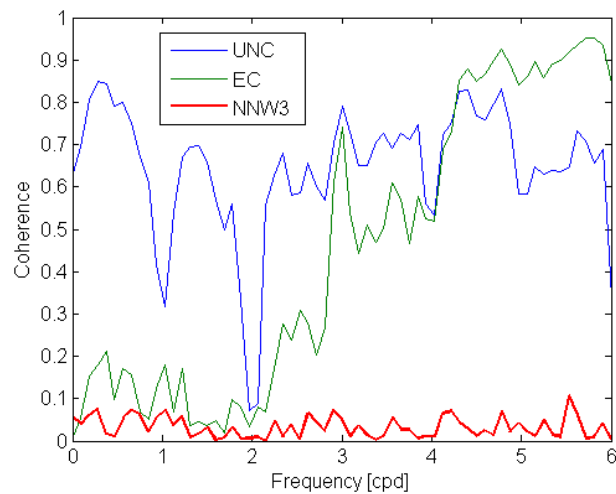


Fig. 6. Coherence between air pressure and tidal residuals obtained by the analysis of uncorrected extensometric data (UNC), data corrected by ETERNA (EC) and data corrected by neural network (NNW3).

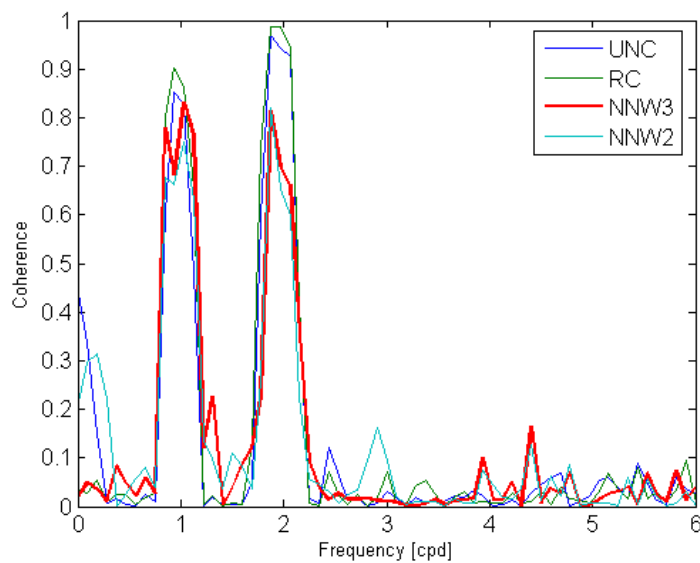


Fig. 7. Coherence between theoretical tide and uncorrected extensometric data (UNC), extensometric data corrected by ETERNA (EC) and neural networks (NNW2 and NNW3).

5. Conclusions

The purpose of this study is to investigate the applicability of neural networks to correct extensometric data for barometric pressure on the basis of local pressure measurements. Three neural networks with different complexity were designed and tested. The first neural network (NNW1) has 3 layers with 4 neurons and non-linear transfer function in the first two layers and a linear transfer function in the last layer. The NNW1 combines 6 hourly pressure data before and after each individual extensometric data to correct extensometric data for barometric pressure. The other two neural networks (NNW2 and NNW3) have 4 layers with 13 neurons in each layer. The NNW2 has linear transfer function in each layer while the NNW3 has non-linear transfer function in the first three layers and a linear transfer function in the output layer. Both neural networks combine 12 hourly pressure data before and after each individual extensometric data.

The results from the effectiveness investigations show that the correction can be made by all of the investigated neural networks. Increasing the complexity of the model the effectiveness of the correction increases only slightly. The best correction was obtained from the NNW3 model.

NNW3 decreased the pressure induced strain amplitudes in the tidal residual by 50% compared to the residual of the simple regression method. While the NNW3 removed the pressure in the whole investigated frequency range the regression method of ETERNA corrected the strain data only in the diurnal and semidiurnal frequency bands.

Correction by neural networks yielded an improvement in the tidal factors relative to the simple regression methods by 2–5% and 30–40% in the semidiurnal and diurnal bands, respectively.

Coherence analysis between theoretical tide and corrected extensometric data resulted in better coherence when strain data was corrected by the ETERNA than when the data were uncorrected, while the coherence was lower in the case of NNW3 correction. The reason for this must be investigated. Probably a further improvement of the NNW3 is necessary.

Investigations show that neural networks can be a useful tool to correct extensometric data for barometric pressure, whereas, in contrast with the simple linear regression models, they can include more air pressure data before and after each individual strain data into the correction than simple regression methods and thus the regional atmospheric effects can be taken into account to some extent on the basis of local atmospheric data.

Acknowledgements

This work was funded by the Hungarian National Research Fund (OTKA) under projects No. K 71952 and K 109060. Special thanks to Ildikó Eperné-Pápai for her help in data preprocessing and Tibor Molnár for his careful maintenance of the instruments.

References

- Boy, J.-P., Hinderer, J., Gegout, P., 1998. Global atmospheric pressure loading and gravity. *Phys. Earth Planet. Inter.* 109, 161–177.
- Boy, J.-P., Longuevergne, F., Boudin, F., Jacob, T., Lyard, F., Llubes, M., Florsch, N., Esnault, M.-F., 2009. Modelling atmospheric and induced non-tidal oceanic loading contributions to surface gravity and tilt measurements. *J. Geodyn.* 48 (3–5), 182–188, doi:10.1016/j.jog.2009.09.22.

- Boy, J.-P., Ray, R., Hinderer, J., 2006. Diurnal atmospheric tide and induced gravity variations. *J. Geodyn.* 41 (1–3), 253–258, doi:10.1016/j.jog.2005.10.010.
- Crossley, D.J., Jensen, O.G., Hinderer, J., 1995. Effective barometric admittance and gravity residuals, *Phys. Earth Planet Inter.* 90, 221–241.
- Crossley, D.J., Hinderer, J., Rosat, S., 2002. Using Atmosphere-Gravity Correlation to Derive a Time-Dependent Admittance. *Bull. d'Inf. Marées Terr.* 136, 10809–10820
- Dehant, V., 1987. Tidal parameters for an unelastic Earth. *Phys. Earth Planet. Inter.* 49, 97–116.
- Demuth, H., Beale, M., 2001. *Neural Network Toolbox for Use with MATLAB, User's Guide, Version 4.* The Math Works, Inc.
- Eper-Pápai, I., Mentés, G., Kis, M., Koppán A., 2014. Comparison of two extensometric stations in Hungary. *J. Geodyn.* 80, 3–11, dx.doi.org/10.1016/j.jog.2014.02.007.
- Farrell, W.E., 1972. Deformation of the Earth by surface loads. *Rev. Geophys. Space Phys.* 10, 761–797.
- Formenti, D., 1999. What is the coherence function and how can it be used to find measurement and test setup problems. *Sound and Vibration, Questions and Answers*, Sage Technologies, Morgan and Hill, California, 2–3.
- Gebauer, A., Kroner, C., Jahr, T., 2009. The influence of topographic and lithologic features on horizontal deformations. *Geophys. J. Int.* 177, 586–602, doi:10.1111/j.1365-246X.2009.04072.x.
- Gebauer, A., Steffen, H., Kroner, C., Jahr, T., 2010. Finite element modelling of atmosphere loading effects on strain, tilt and displacement at multi-sensor stations. *Geophys. J. Int.* 181, 1593–1612, doi: 10.1111/j.1365-246X.2010.04549.x.
- Hartmann, T., Wenzel, H.G., 1995. The HW95 tidal potential catalogue. *Geophys. Res. Lett.* 22, 3553–3556.
- Klügel, T., Wziontek, H., 2009. Correcting gravimeters and tiltmeters for atmospheric mass attraction using operational weather models. *J. Geodyn.* 48 (3–5), 204–210, doi:10.1016/j.jog.2009.09.01.
- Kroner, C., Jentzsch, G., 1999. Comparison of different barometric pressure reductions for gravity data and resulting consequences. *Phys. Earth Planet. Inter.* 115, 205–218.
- Latynina, L.A., Vasil'ev, I.M., 2003. The Earth surface deformations caused by air pressure variations. *J. Geodyn.* 35, 541–551, doi:10.1016/S0264-3707(03)00013-9.
- Mentés, Gy., 2010. Quartz tube extensometer for observation of Earth tides and local tectonic deformations at the Sopronbánfalva Geodynamic Observatory, Hungary. *Rev. Sci. Instrum.* 81, 074501, doi:10.1063/1.3470100.
- Merriam, J.B., 1992. Atmospheric pressure and gravity. *Geophys. J. Int.*, 109, 488–500.
- Müller, T., Zürn, W., 1983. Observations of Gravity Changes During the Passage of Cold Fronts. *J. Geophys.* 53, 155–162.
- Niebauer, T.M., 1988. Correcting gravity measurements for the effects of local air pressure. *J. Geophys. Res.* 93 (B7), 7989–7991.
- Neumeyer, J., Hagedoorn, J., Leitloff, J., Schmidt, T., 2004. Gravity reduction with three-dimensional atmospheric pressure data for precise ground gravity measurements. *J. Geodyn.* 38, 437–450.
- Räbel, W., Zschau, J., 1985. Static deformations on gravity changes at the earth's surface due to atmospheric loading. *J. Geophys.* 56, 81–99.
- Spratt, R.S., 1982. Modelling the effect of atmospheric pressure variations on gravity. *Geophys. J. R. Astr. Soc.* 71, 173–186.
- Steffen, H., Kuhlmann, S., Jahr, T., Kroner, C., 2006. Numerical modelling of the barometric pressure-induced noise in horizontal components for the observatories Moxa and Schiltach. *J. Geodyn.* 41 (1–3), 242–252, doi:10.1016/j.jog.2005.08.011.

- van Dam, T.M., Altamimi, Z., Collilieux, X., Ray, J., 2010. Topographically induced height errors in predicted atmospheric loading effects. *J. Geophys. Res.* 115, B07415, doi:10.1029/2009JB006810.
- van Dam, T.M., Blewitt, G., Heflin, M.B., 1994. Atmospheric pressure loading effects on Global Positioning System coordinate determinations. *J. Geophys. Res.* 99 (B12), 23,939–23,950.
- van Dam, T.M., Wahr, J., 1987. Displacements of the Earth's Surface Due to Atmospheric Loading: Effects on Gravity and Baseline Measurements. *J. Geophys. Res.* 92 (B2), 1281–1286.
- van Dam, T.M., Wahr, J., Chao, Y., Leuliette, E., 1997. Predictions of crustal deformation and of geoid and sea-level variability caused by oceanic and atmospheric loading. *Geophys J. Int.* 129, 507–517.
- Warburton, R.J., Goodkind, J.M., 1977. The influence of barometric pressure variations on gravity. *Geophys. J. R. Astr. Soc.* 48, 281–292.
- Wenzel, H.G., 1996. The nanogal software: Earth tide data processing package ETERNA 3.30. *Bull. d'Inf. Marées Terr.* 124, 9425–9439.
- Wunsch, C., Stammer, D., 1997. Atmospheric loading and the oceanic “inverted barometer” effect. *Rev. Geophys.* 35 (1), 79–107.

BLANK PAGE